We are IntechOpen, the world's leading publisher of Open Access books Built by scientists, for scientists

6,900
Open access books available

185,000
International authors and editors

200M
Downloads

Our authors are among the

154
Countries delivered to

TOP 1%
most cited scientists

12.2%
Contributors from top 500 universities

WEB OF SCIENCE™

Selection of our books indexed in the Book Citation Index in Web of Science™ Core Collection (BKCI)

Interested in publishing with us?
Contact book.department@intechopen.com

Numbers displayed above are based on latest data collected.
For more information visit www.intechopen.com

11

Plasma Based Dry Release of MEMS Devices

Hamood Ur Rahman
College of Electrical and Mechanical Engineering
National University of Sciences and Technology (NUST)
Islamabad,
Pakistan

1. Introduction

Microelectromechanical Systems (MEMS) are constructed to achieve a certain engineering function or functions by electromechanical or electrochemical means. Very intricate moveable structures can be fabricated using the sacrificial layer (Madou, 2002). These moveable suspended structures are micro-bridges fabricated using the sacrificial layer. These structures can be cantilever beam bridges fixed at one end or membrane bridges fixed at both ends. In the field of RF MEMS these two types of bridges are used to fabricate the series or shunt switches.

In a fabrication process, the final release of a MEMS device is the most crucial step. Surface micromachining process relies on both wet and dry etching techniques. Wet etching has been widely used for pattern delineation. In wet etching, liquid etchant dissolves away the exposed film and attacks isotropically, resulting in loss of pattern definition due to undercutting and rounding of film features. This chapter suggests a solution to the problem of stiction by avoiding the wet release and in the absence of Critical Point Dryer (CPD). A dry release technique is presented for the RF MEMS structures, that combines the removal of sacrificial layer through wet etching and its substitution with standard photoresist. After coating, this photoresist acts as a supporting layer under the structure and rejects the structure to attack the substrate (Orpana & Korhonen, 1991). During this complete process wafers are not allowed to dry at any moment of time, otherwise structures may be permanently bonded with the substrate. The supporting layer is removed by oxygen plasma using the Reactive Ion Etching (RIE). In the dry etching, residual waste is off concern which effect the reliability of the MEMS structures. Motivation for this unique process was that some left over residues were observed after the single step or traditional RIE process. Secondly, this process was more cost effective as compared to a wet release CPD technique using CO_2 dryer. The process not only produced less residual waste but achieved a clean dry release.

2. Need for dry etching

A serious limitation of suspended MEMS structures is that they tend to deflect through stress gradient or surface tension induced by trapped liquids during the final rinsing and drying step. Problems like stiction and bridge collapse are associated with producing a free standing structure. The stiction is described as a process of bonding the top and bottom

electrodes together by a microscopic surface due to the planner nature of the electrodes. Stiction of MEMS is a common concern. When a sacrificial layer is removed and rinsed in deionized water, the surface tension of rinse water pulls the delicate micro structure to the substrate as the wafer dries. Risk of stiction is caused by the capillary forces originating from the dehydration of meniscuses, van der Waals force or the electrostatic force formed between the suspended beam structures and the substrate following the wet etching (Madou, 2002). These forces keep the structure firmly attached with the substrate. Stiction remains a reliability issue due to contact with adjacent surfaces after release.

Stiction is an inevitable problem we deal with for achieving the working RF MEMS devices. With increase in cantilever length, its flexibility perpendicular to the substrate increases which also increases the susceptibility to stiction. When the structure gets attached with the substrate due to stiction, the mechanical force required to dislodge it from the surface is large enough resulting in damage to MEMS structure (Modou, 2002). The surface morphology has a strong influence on stiction and is a serious problem particularly in metal to metal contact switches (Varadan et al., 2003).

In order to achieve a released structure, contact between the structural elements and the substrate should be avoided during processing. Etching can be done by physical damage, chemical damage or combination of both. Release of these suspended beam structures can be done either through wet etching or dry etching. Etching in a plasma environment has several advantages as compared to wet etching. In the wet etching, this may become impossible or very difficult due to large surface tension forces. Moreover, if a MEMS structure is left too long in the etchant, the structure can be over etched and damaged (Harsh et al., 1999). Plasmas are easier to start and stop than simple immersion wet etching (Campbell, 1996). Also sensitivity of plasma etch is less prone to small changes in the temperature of the wafer. Above mentioned factors make plasma etching more repeatable than wet etching.

Different techniques over a period of time have been used to avoid stiction. Method of creating stand-off bumps on the underside of a polysilicon plate was introduced (Abe et al., 1995) which added meniscus shaping microstructures to the perimeter of the microstructure for reducing the chance of stiction. To avoid stiction critical point drying technique using CO_2 dryer is used (Chan et al., 2007) to release the structures.

3. Mitigation of stiction

3.1 Causes of stiction

The gap between two metal surfaces or device to substrate is so small that strong capillary forces can be developed during the dehydration which may lead to the adhesion of two surfaces. The same adhesion can occur when device is exposed to high humid conditions which lead to capillary condensation. Microstructures which contaminate the contact surface if stiction occurs, are in fact the synthetic particles of the metals (Alley et al., 1992).

The adhesion may occur due to solid bridging or liquid bridging. In solid bridging, the non volatile impurities present in the drying liquid are deposited on solid surfaces if drying by evaporation is conducted. These impurities may be introduced due to dissolution of the particles or substrate materials by liquid or through dissolution of residues distributed uniformly on the surface of the substrate. The deposition of impurities is pronounced in narrow spaces and between the two metal contacting surfaces upper and lower. This results in adhesion between the metal surfaces. The adhesion strength through solid bridging is

difficult to estimate because of the variation in deposition process or the density of deposited material. In any case, the adhesion strength tends to be significant.
The liquid bridging occurs due to the surface tension of the trapped capillary liquids. The drying of this trapped liquid is difficult due to the presence of concentrated soluble impurities. These trapped impurities increase surface tension while decreasing the vapor pressure. A third possible adhesion cause can occur if suspended membrane is placed in contact with the lower contact surface due to some external force. This adhesion can occur due to deliberate placement of collapsing forces or can be due to shock effect (Mastrangelo, 2000).

3.2 Stiction due to capillary forces

The removal of sacrificial layer to achieve a suspended microstructure is the final step in the surface micromachining process. This process mostly requires a wet etching for removal of sacrificial layer. In some cases the removal is also done using plasma etch when sacrificial layer is other than a metal layer like polyimide or photo-resist. After the wet etching the microstructure is rinsed using DI water to remove the residues left during the etching. When the microstructure is pulled out of DI water a strong capillary force develops. A meniscus forms at the interface under the microstructure when the microstructure is pulled out of water. The curved interface creates a pressure called Laplace pressure which is given by (Israelachvili, 1991)

$$P_L = \gamma_l \left(\frac{1}{r_a} + \frac{1}{r_b} \right) \tag{1}$$

The liquid surface tension is denoted by γ_l and two radii of curvature of liquid surfaces are given as r_a (parallel to surface normal of the substrate) and r_b (in the plane of the substrate). In most cases, the liquid droplet on the surface of the substrate will not wet it. It will present a definite angle of contact between the liquid and the substrate as shown in figure 1.

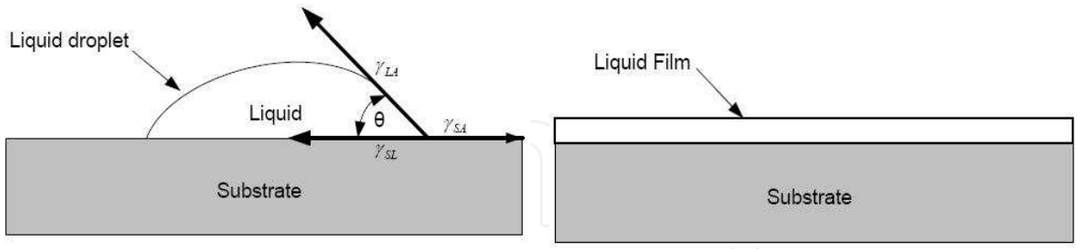

(a) (b)

Fig. 1. Contact angle at solid liquid interface of (a) non-spreading (b) spreading liquid

In equilibrium condition, the contact angle between liquid and solid is determined by the balance between the surface tension of the three interfaces. The contact angle θ at the junction of three interfaces is defined as the angle formed between solid-air, liquid-air and liquid-solid interfacial tensions in equilibrium. The contact is given by the Young's equation (Israelachvili, 1991) as

$$\gamma_{SA} = \gamma_{SL} + \gamma_{LA} cos\theta \quad 0 < \theta < \pi \tag{2}$$

If the γ_{SA} surface tension is smaller than the sum of γ_{SL} and γ_{LA} surface tensions, then the contact angle is larger than 0^0 and liquid will be non spreading as shown in figure 2(a). If the γ_{SA} surface tension is larger, than the sum of γ_{SL} and γ_{LA} surface tensions, it will spread the liquid energetically. Then the contact angle is equal to 0^0 and liquid will spread thus forming a drop bridging between the two surfaces as shown in figure 2(b). The total surface energy of the area between the metal contacting parts can be calculated by adding the surface tensions of all the three interfaces (Mastrangelo & Hsu, 1993).

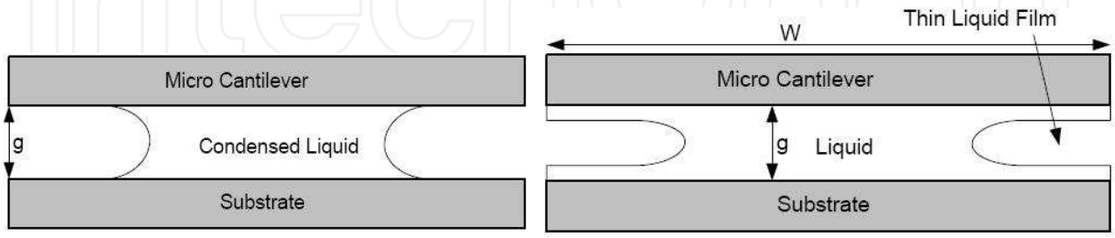

(a) (b)

Fig. 2. The capillary condensation phenomenon of (a) non-spreading (b) spreading liquid showing underneath of a cantilever beam (front view)

Because the lateral dimesions of microstructures like cantilever beams are much larger than the vertical gap spacing (g) due to liquid layer thickness, i.e. $r_b \gg r_a$, therefore we may write (1) as,

$$P_L = \frac{2\gamma_l \cos\theta}{g} \tag{3}$$

where θ is the contact angle of the liquid at the surface of the substrate and g is the gap height between the cantilever and the substrate which is equal to $2r_a \cos\theta$.

The shape of the meniscus will be concave ($r_b < 0$) under a cantilever structure on a hydrophilic surface (silicon or any metal) which forms a quite shallow contact angle i.e., $\cos\theta \approx 1$ as shown in figure 2(a), so the resulting Laplas pressure is negative. This will create sufficient attractive capillary force that will pull the cantilever beam structure down into contact with lower metal surface or substrate as shown in figure 3. Hence the cantilever beam falls into adhesion or stiction with substrate or metal surface following the drying process.

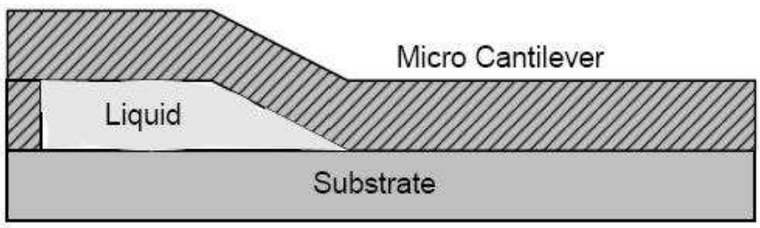

Fig. 3. The process of the microstructure drying that leads to the adhesion of micro cantilever to adjacent surfaces

The stiction between the two metal surfaces due to capillary forces looks quite similar to solid bridging. In the solid bridging, nonvolatile impurities are deposited on the solid surface causing the adhesion during the drying whereas in the capillary forces adhesion of a thin liquid layer works as an adhesion force between the two solid surfaces. If the contact angle θ between the solid and liquid is less than 90^0 (figure 2(a)) then the pressure inside the liquid drop will be less than outside. This results in a net attractive force between the two contacting plates. Figure 4 shows the SEM image of the cantilever beam structure stuck with lower metal surface due to capillary force. The adhesion of the beam was strong. An attempt was made to release the front part of the cantilever using micro probe. This resulted in breaking of the cantilever beam.

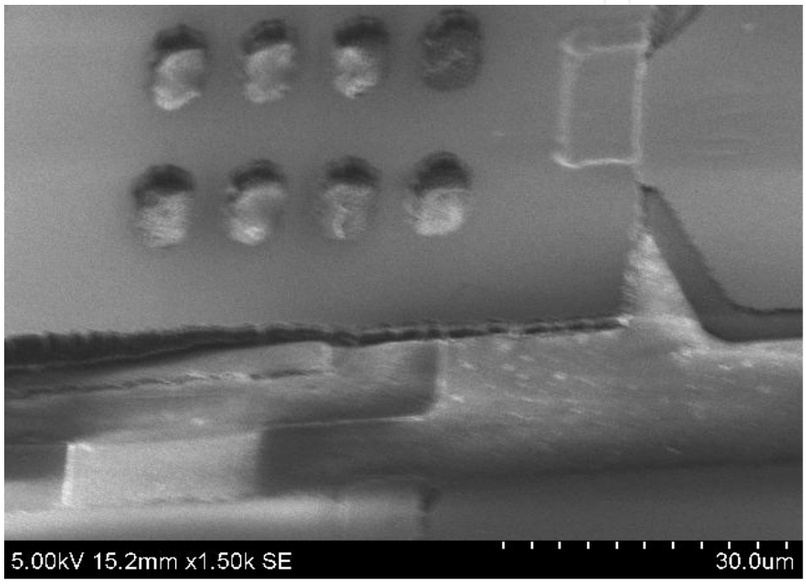

Fig. 4. SEM of cantilever beam held with stiction due to capillary forces

3.3 Drying method of cantilever beams

In this study, fabrication of RF MEMS is done using the CPW structure. When liquid attaches to the long cantilever beam, separation between the beam and CPW is a function of position whereas gap is smaller near the tip than near the anchor. As $r_a \rightarrow \infty$, the radius r_b remains constant as the droplet pressure is constant. As the liquid dries, the decrease in surface area drives the radius r_b to smaller values. The droplet will form an inside meniscus near the base which forces the droplet to neck down in this region resulting in a negative value of r_a. The necking continues with lower negative value of r_a until the two meniscuses on either side of the beam meet and pinch off a separated droplet. This technique for drying of water activates the capillary forces which can lead to adhesion. However, for applications discussed here the drying method has been used while avoiding the meniscus so that capillary force does not come into play at the time of drying.

In this drying method, the sacrificial layer was removed by wet etching. During rinsing with DI water when capillary forces could act for stiction during drying, we dipped the device in acetone till the time whole water under the cantilever beam was removed. The acetone dip also removed the diluted impurities which were present in the DI water while removing the

sacrificial layer. Drying does not takes place with acetone, but device was dipped into a thin photo-resist (AZ5214E) which took a place underneath the cantilever beam as a supporting layer. The acetone evaporates quickly, therefore at no stage sample was exposed to the air. The photo-resist became a concentrated resist as the acetone evaporates leaving only the supporting layer of photo-resist. Now drying of photo-resist with hard-bake will remove the solvents from the photo-resist and then etch the photo-resist supporting layer with O_2 plasma using RIE. This drying method resulted in clean surface without residues and no stiction was observed during the process.

3.4 Stiction by contact adhesion

Another phenomenon which can produce adhesion between the two surfaces is an inter-solid adhesion which can overcome the restoring force of the elastic beam. Figure 5 shows the cross section of a cantilever beam with length *L*, width *W*, height *g*, and thickness *t*. The Young's modulus of the beam is represented by *E* which is 78GPa in terms of Au metal used for the fabrication of the switch. The figure shows that beam is adhering to the substrate at a distance $d = (L-x)$ from its tip.

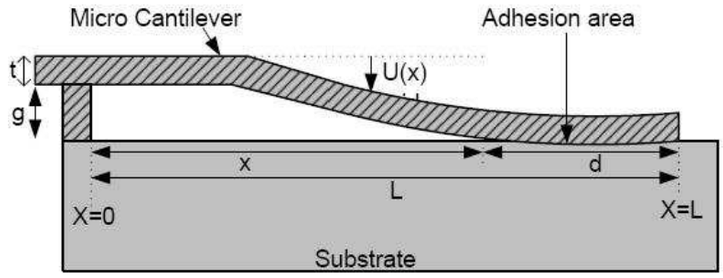

Fig. 5. Schematic of a cantilever beam adhering to the substrate

We can calculate the total energy of the system which is sum of the elastic and surface energies and is given (Mastrangelo, 2000) by

$$U_T = U_E + U_S = \frac{6EIg^2}{x^3} - \gamma_s W d \tag{4}$$

where U_E is the bending energy stored in the beam and U_S is the interfacial energy of the contact area. Shear deformations are particularly important for $x \rightarrow L$, as $d = (L-x)$ is very small and tip of cantilever beam changes its elastic energy substantially just before detachment. This causes the beam to detach from substrate (Mastrangelo &Hsu, 1993) when $L = x = (3Et^3h^2/8\gamma_x)^{1/4}$ where γ_x is the surface energy which is determined from the detachment length and beam dimensions.

3.4.1 Inter solid adhesion reduction method

To eliminate the chance of permanent adhesion failure between the two solid surfaces, an inter-solid surface adhesion reduction is required. This can be done using techniques such as use of textured surfaces and posts, low energy molecular coatings and fluorinated coatings. The textured surfaces and posts approach has been used for the method presented here. Contact area between the elastic cantilever beam and the lower metal contact area on substrate was reduced which in turn reduced the adhesion forces.

The surface roughness of the upper contact area and lower contact area is rough enough, thus generates a rough interface between the two contact areas. The measured surface roughness of the upper contact area is 18nm and lower contact area is 22nm, respectively. This accomplishes the texturing of contact surfaces.
Texturing of the two solid surfaces was enhanced deliberately by introducing the construction of a small supporting post. In this approach, a dimple was introduced under the front tip of the cantilever. The dimple was constructed by making an extra mask layer in the fabrication process before patterning the cantilever beam. The dimensions of the dimple are 10×20μm with the height 0.9μm. Figure 6 shows the SEM of the dimple. It was taken by manually turning the cantilever beam using a lift out microscope.

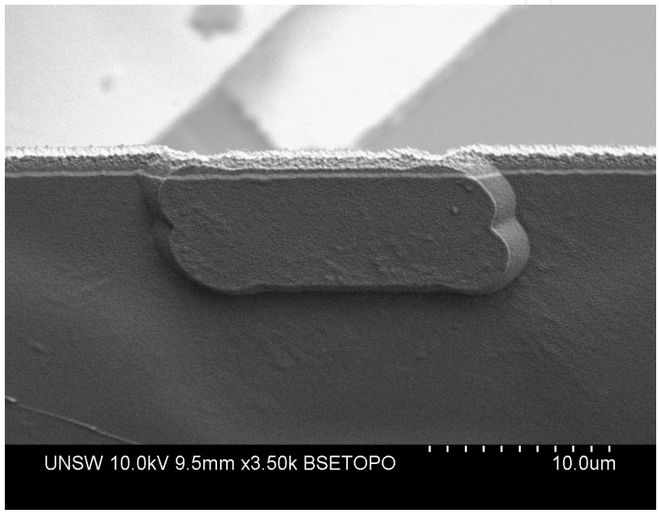

Fig. 6. SEM of the dimple under the front end of the cantilever beam

The contact adhesion was also investigated by using a sharp Tungsten probe tip. The radius of curvature of the probe tip was 1μm. The sharp tip of the probe was used to pull the beams down under a high magnification microscope to ensure that cantilever tip has made contact with lower surface. When the tip of the cantilever touched the lower CPW surface, the probe tip was removed and cantilever beam started peeling off the surface. During this experimentation, there were only two options available to verify that either the beam would stick to lower surface or the beam would come off without stiction. A number of samples were tested after the release and no inter-solid adhesion was observed in these samples.

4. Dry etch process optimization using RIE

The first batch of wafers was used to optimize the release of the final device. For this purpose whole fabrication process was skipped and only the mask layers which were required for the fabrication of cantilever beams were used. For optimizing the release process Aluminum (Al) metal was used as it was readily available rather than expensive Au metal. Once the release process was carefully optimized, Au layer was used for the final fabrication of RF MEMS switches.
A 2.5μm thick layer of photo-resist (AZ6612) was deposited and then patterned for anchor. A 1.5μm thick layer of evaporated Al was deposited using e-beam evaporator. A layer of 1.0μm of photo-resist was deposited to pattern the cantilever beam. Two approaches were

used to dry release the cantilever beams. First, one wafer was used to directly dry etch the sacrificial layer of photo-resist without using any other process on it. In this approach, it was observed that RIE tool was not able to remove the sacrificial layer material sufficiently from the devices. Some leftover metal residues were also observed which could not be cleaned even after extensive DI water rinsing of the wafer. A prolonged exposure of anisotropic RIE also damaged the cantilever beam structures.

In the second approach, a combination of wet and dry release was used to remove the leftover metal residues after etching while replacing a new layer of photo-resist as a supporting layer. The sample was inspected under microscope followed by SEM and in this case metal residues were not observed on the sample or supporting layer. Wafer was exposed under O_2 plasma in RIE chamber for dry etch. The wafer was exposed to high RF power (70W) and high pressure (30Pa). The high RF power generated an intense bombardment of plasma atoms with high pressure.

Devices were inspected under the microscope after the first etching exposure. It was observed that although plasma etched the photo-resist from top and sides of the device a significant amount of resist was observed under the cantilever beam. A second exposure of plasma was given again to the samples. After second exposure of plasma it was observed that resist was still visible under the beam. However, the beam structures were discoloured. It was assumed that some resist was still on the beam which created this discolourization. However, when the samples were observed under SEM, it showed that this discolourization was not due to resist but the beam structures were damaged due to high power plasma particles.

Figure 7(a) shows the SEM image of bridge over bias line with damaged surface. A metal peeling from some parts of the bridge is also visible. One can observe that high power bombardment of plasma atoms has damaged the metal layers on the device. Figure 7(b) shows the cantilever beam structure damaged due to RIE plasma while optimizing the release process.

After a number of iterations, it was revealed that power and pressure were the main factors for the optimization of dry release process. Variation of power and pressure from high to low and vise versa can change the plasma behavior inside the chamber. The voltage bias was also controlled once these parameters were changed. With high RF power and low pressure we achieved a bias of 232±6V which indicated that plasma particles generated inside the chamber strike the surface of the substrate with more power giving anisotropic etching behavior. With low power and high pressure the bias changed to as low as 90±6V which changed the plasma atoms behavior from anisotropic to isotropic giving etch profile below the surface of the cantilever beam also.

Three wafer samples were used to optimize the RIE process using the supporting layer technique. In this case, a careful shifting of power and pressure parameters was done. Once sample was ready with supporting layer of photo-resist underneath the cantilever beam, the sample was exposed to high power and low pressure for one hour. In this case, the plasma particles struck the wafer surface with high power but under low pressure. It did not damage the device surface. The sample was observed under the microscope and a significant amount of photo-resist was observed on the sample as well as under the beam. The sample was exposed to plasma for 30min and then inspected again under microscope. It was observed that much of the resist from top of the beam and sides was removed but a small amount of resist was still visible on the beam and significant amount of resist was observed under the beam. Sample was exposed to another 30min exposure which cleaned

the resist from top and sides of the beam but under the beam resist was observed. Now, the power and pressure parameters of the RIE tool were changed from high power to low power and from low pressure to high pressure. This created an isotropic behavior of the plasma instead of anisotropic behavior which was observed in the first setting. Sample was exposed to plasma for one hour which resulted in a clean release of the structures.

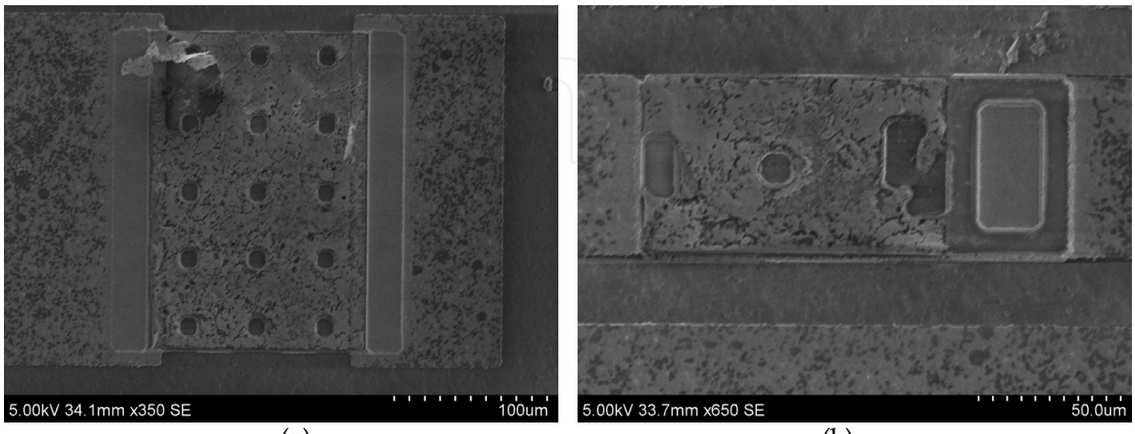

(a) (b)

Fig. 7. SEM of discolored/damaged areas after RIE (a) bias line bridge (b) cantilever beam

5. Fabrication process

The fabrication of the RF MEMS switches is a six mask all metal fabrication process, as shown in figure 8. All processing steps are developed on the basis of standard CMOS processing. A standard one-layer photo-resist was used as a mask during the fabrication process to provide precise pattern definition. However, during release step the photo-resist was also used as a sacrificial layer. The photo-resist (AZ6612) was a positive photo-resist sensitive to ultraviolet (UV) radiation and can be developed with AZ-300 MIF solution. Throughout the fabrication process, alignment was performed with Quintal Q-6000 mask aligner with UV light exposure. In order to achieve good RF performance device, the switch was fabricated on a low loss alumina substrate with dielectric constant 9.9.

The fabrication is a six mask all metal process. The process started with the standard wafer cleaning process. DC bias lines and actuation pads were defined by evaporating 0.04μm layer of Cromium (Cr). This layer was then patterned with mask one. The Cr metal evaporation was done using Lesker evaporator operating in 10^{-6} Torr range. An insulator layer in a series switch served as a mechanical connection as well as electrical isolation between the actuator and the contact. Since the switch was made of metal, the insulator layer also acted as a dielectric layer which was needed to prevent direct contact between the metal cantilever bridge and the actuation pad.

A 0.75μm thick layer of silicon nitride was deposited as dielectric layer using PECVD and patterned with mask two. The deposition of Si_3N_4 was performed using VACUTEC-1500 series PECVD equipment. The CPW lines were defined by evaporating/RF sputtering of 0.04/1.0μm thick layer of Cr/Au and patterned with mask three. Cr was used as an adhesion layer between the Au and substrate. The sputtering was performed using Edwards E-306 series sputtering tool which was used for RF sputtering of the Au film.

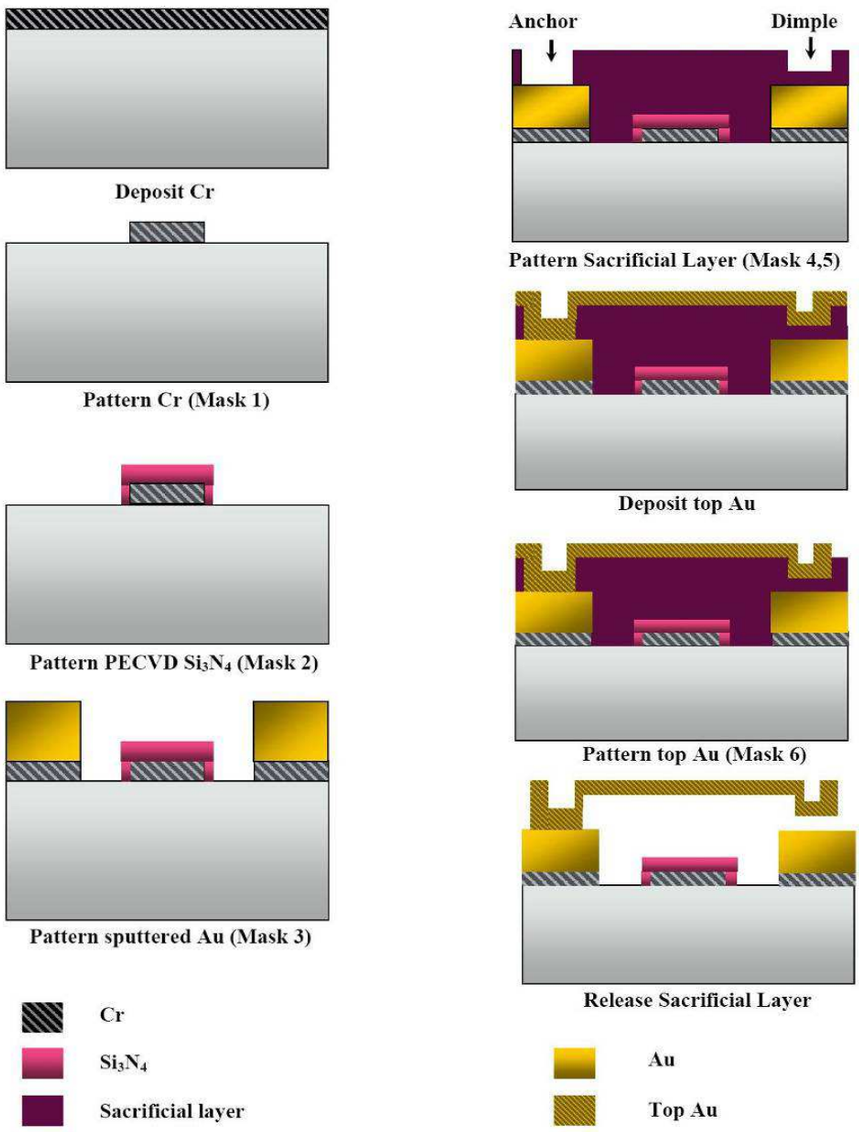

Fig. 8. Six mask fabrication process for RF MEMS switches

Then a 2.5µm thick layer of photo-resist (AZ-6632) was deposited as sacrificial layer and patterned for anchor and dimple with mask four and five respectively. While defining the anchor and dimple full dark masks were used to expose only the anchor and dimple areas. This was followed by a 1.5µm thick layer of RF sputtered Au which was patterned with mask six to form the cantilever beam. Finally, the bridge structure was released using a unique dry release process.

6. Dry release process

During fabrication of RF MEMS switches both dry and wet release methods were applied. The yield of wet release was very low and no working prototype was achieved. Problems related to wet release and stiction have already been discussed in the previous sections. As

explained in last section, in single dry release process, the problem of left over residues of metal after etching the metal layer was experienced. So a unique dry release process was developed with a combination of wet and dry release to achieve better results.

6.1 Dry release model

Motivation for this unique process was that some left over residues were observed after the single step or traditional RIE process. Secondly, this process was more cost effective as compared to a wet release CPD technique using CO_2 dryer. The process not only produced less residual waste but achieved a clean dry release. The steps for dry release process are described in figure 9.

First, the sacrificial layer was removed using acetone. This also included the removal of some Au leftover residues on photo-resist from the previous wet etching with mask 6 [figure 9(a)]. After this, sample was dipped again into clean acetone for 30 min for final cleaning. Then the structure was immediately dipped into another resist (AZ5214E), until all the liquid covering the sample was concentrated resist [figure 9(b)] (Forsen et al., 2004 & Orpana & Korhonen, 1991). The resist covered sample was spun at 2500 rpm to achieve uniform layer of resist and then soft backed at 90ºC resulting in a thick layer of photo-resist fully encapsulating the suspended beam as a supporting layer.

It must be noted that the wafer was never allowed to dry during the the process or else structure would be permanently bonded to the substrate. The structure was then dry released by Oxygen plasma using the single process RIE in two steps. In step one the etching was done using high power and low pressure (15sccm O_2, 180 W, 8 Pa) giving an anisotropic etch of the photo-resist [figure 9(c)]. In step two low power and high pressure (15sccm O_2, 50 W, 40 Pa) was used. This resulted in isotropic etching of the photo-resist thus giving a free standing structure at the end [figure 9(d)].

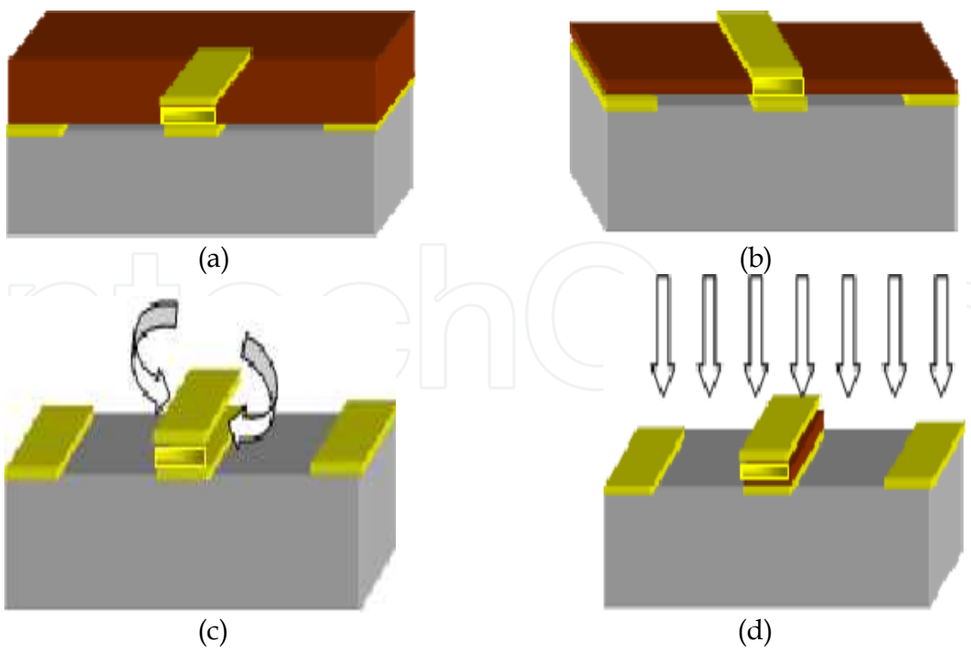

Fig. 9. Schematic representation of process steps involved in dry release process of MEMS structures (a) patterned cantilever beam over sacrificial layer of AZ-6612 (b) cantilever beam dipped in structural layer of AZ-5214E (c) anisotropic etching (d) isotropic etching

6.2 Dry release using RIE

Figure 10 displays a SEM image of the fabricated switch. The sacrificial layer (AZ-6612) has been removed after two dips in acetone; supporting layer below the structure has been made with another photoresist (AZ5214E). It can be observed that structure has got a clear standing on the supporting layer. There is no indication of left over residues of the Au after acetone cleaning.

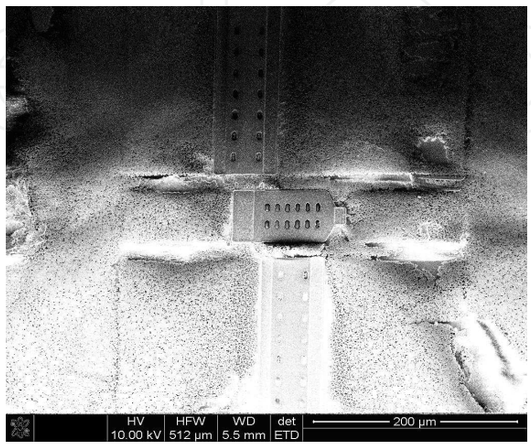

Fig. 10. SEM of the RF MEMS switch with supporting layer

Figure 11 shows a SEM image of the structure after anisotropic etching during the first step of single process RIE. The structure rests on supporting layer. Some leftover parts of the chemical waste are also visible. The chemical waste observed during the dry etching was comparatively less than as seen in the wet etching.

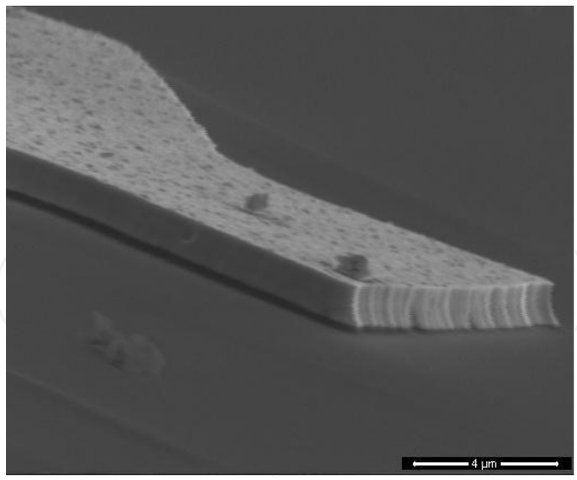

Fig. 11. SEM of the cantilever beam structure resting on supporting layer after anisotropic etch

During the isotropic etching step of RIE, plasma moves in all directions and etches the photo-resist layer located below the cantilever beam structure. Figure 12 shows the released RF MEMS cantilever beam structures. The clean standing structure of the MEMS bridge can be observed. The release of structure was clean and results achieved by this process technique were satisfactory.

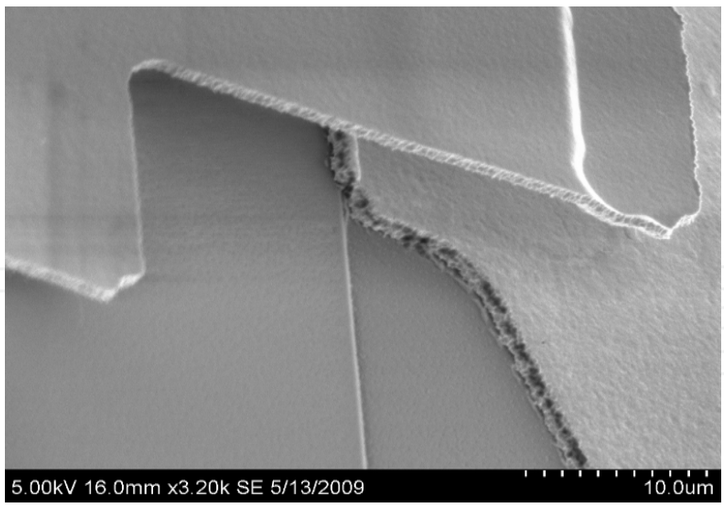

Fig. 12. Released RF MEMS switch cantilever beam (front tip view)

From the SEM images and optical microscopy it was observed that the released beam structure showed higher curling up trend. This was due to residual gradient stress in the film and lead to the increase in the actuation voltage. The stress gradient lead to the lift of beam around 1µm after the release of structure. The measured lift of cantilever front end is 4.3µm after release. Figure 13 shows a DEKTAK profile of the unreleased and released beam tip of RF MEMS switch. In figure 13(a) DEKTAK profile indicates the beam height after patterning mask six which also confirms the gap height distance of 2.5µm. When beam structure was released using RIE plasma technique, the lift of the front tip of the cantilever beams was measured again which confirms the curling up trends of the beam stated above.

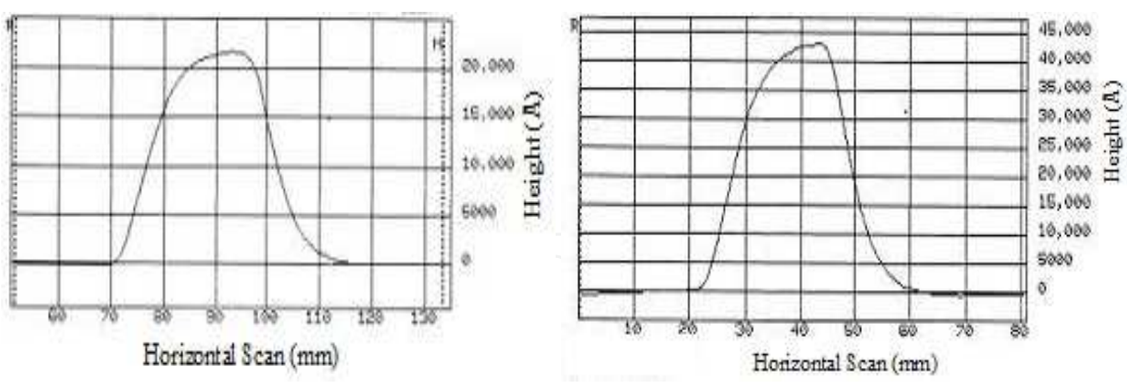

(a) (b)

Fig. 13. DEKTKK image of beam tip (a) before release (b) after release

6.2.1 Yield

The yield of the released structures on the wafer was measured using visual examination and SEM. No stiction was observed with new release process. However presence of some residues was observed on the outer samples of the substrate. This was due to non uniform plasma distribution during the RIE. The yield of the release process was worked out on full cleaned samples. A yield of more than 70% was achieved with contact resistance of less than 2.7Ω.

7. Fabricated RF MEMS switches

Due to better flexibility for large systems and wide band applications, metal to metal contact switch was chosen over the capacitive switch. The CPW centre conductor was 60μm wide, 20μm gap and 210μm ground widths which resulted in characteristic impedance of 50Ω. The beam was suspended 2.5μm from the substrate. The ground planes around the beam were suspended as it provided easy access to beam and electrode when being used in biasing systems. The switches were fabricated using the developed six mask all metal process. A dimple was used at the bottom of front centre tip of the cantilever beam to reduce the stress sensitivity of the beam. Front tip contact area was small as compared to conventional cantilever beams because of following reasons. First, small contact points would reduce the metal-to-metal stiction and would increase the contact pressure. Secondly, it gave better isolation.

Figure 14 displays the proposed arrow beam design. The length of the beam is 120μm and the width of the beam is 60μm. The beam has been curved inside from the front with a front tip 20μm in width.

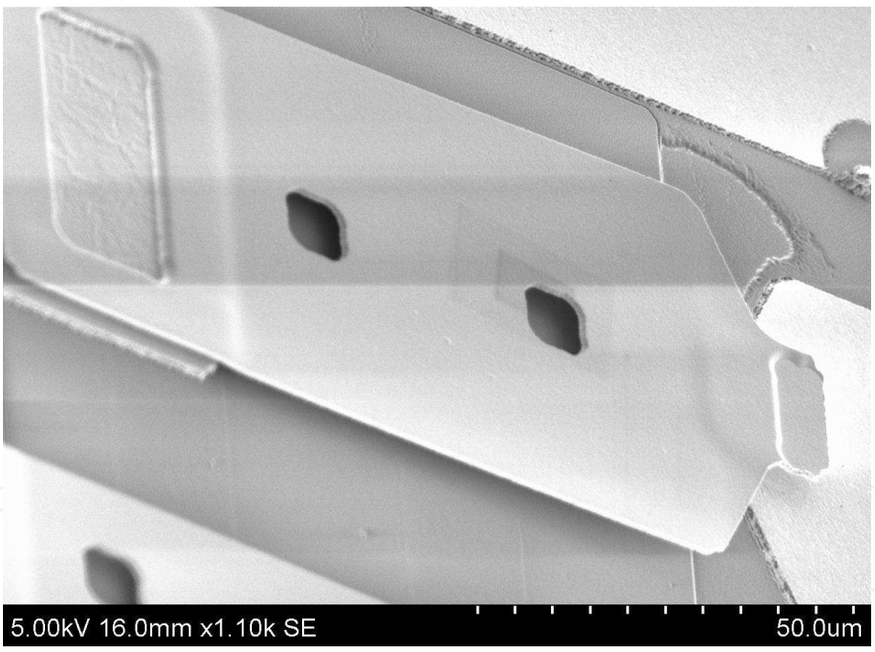

Fig. 14. SEM of fabricated arrow beam cantilever based RF MEMS switch

Figures 15 and 16 show the two proposed cantilever beam designs. In figure 15, the beam labeled Design-1 has three supported cantilever bars which behave like three springs while moving the beam during the actuation. The length of each cantilever bar is 20μm and the width is 10μm. The gap between each cantilever bar is 15μm and provides symmetry to the beam structure. All three cantilever bars are connected with an anchor which is 20μm in length and 60μm wide. The supported cantilever bars are then connected with a beam of length 100μm and width of 60μm.

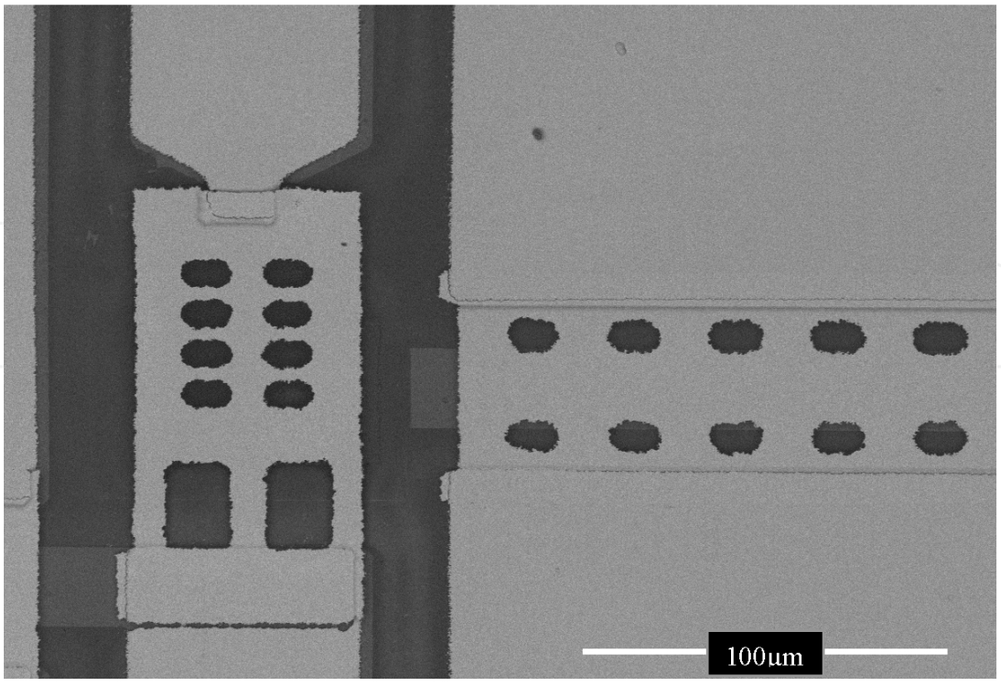

Fig. 15. SEM of fabricated RF MEMS switch

Figure 16 shows the beam labeled Design-2, with three supported cantilever bars and an extended cantilever at the front. The dimensions of the three supported cantilever beams are the same as that for Design-1, with the centre 60µm×60µm and the extended cantilever at the front 40µm×20µm.

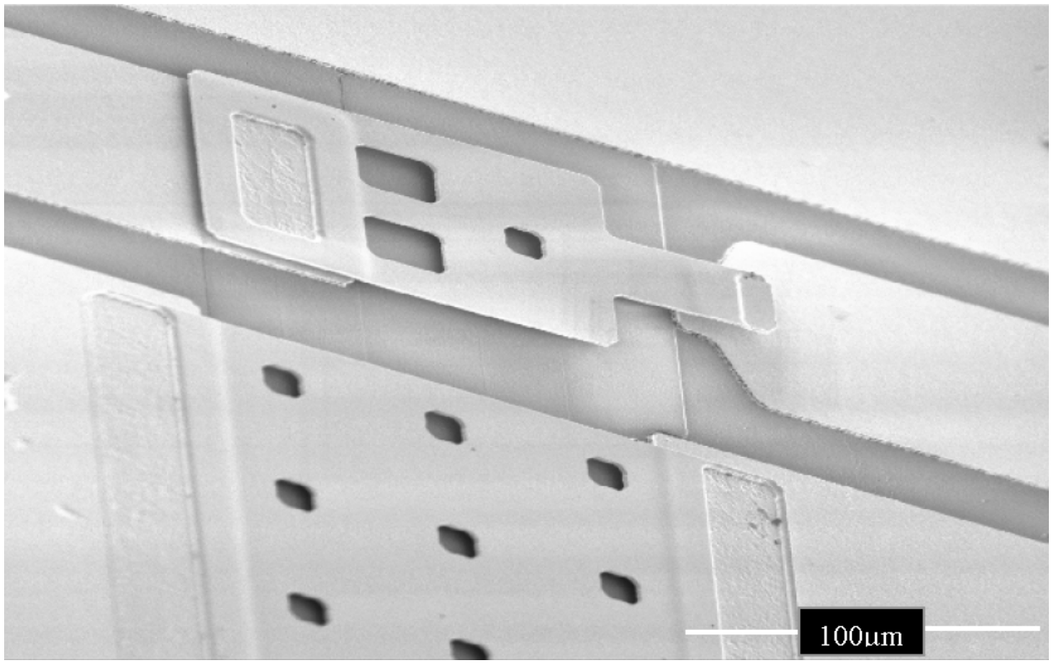

Fig. 16. SEM of fabricated RF MEMS switch

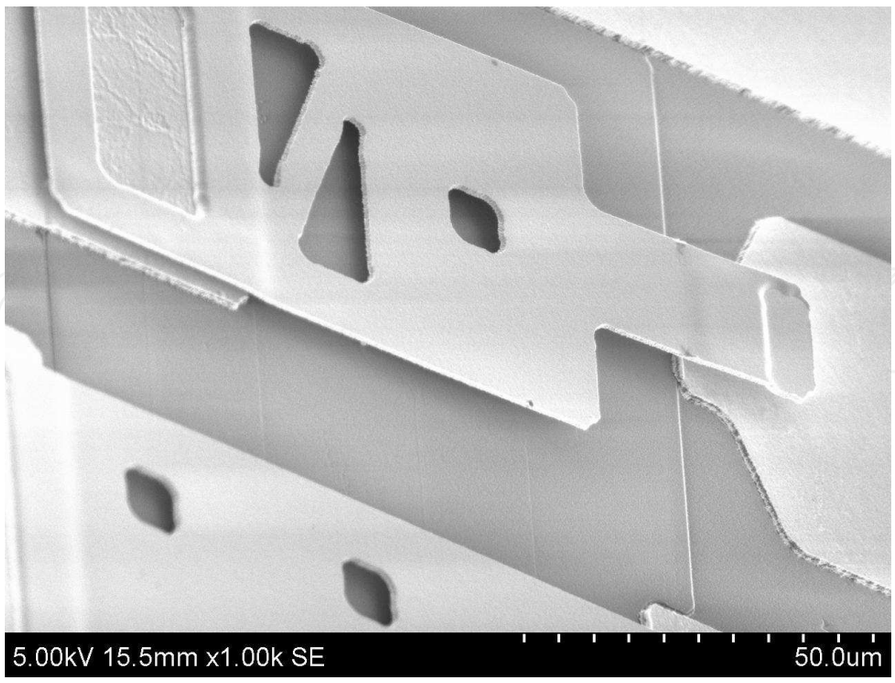

Fig. 17. SEM of fabricated RF MEMS switch

Figure 17 shows the RF MEMS switch which has the same dimensions of beam as explained in figure 16, instead of three supporting bars, has two supporting bars with a single cross bar link intended to increase the strength of the two low spring constant supporting bars.

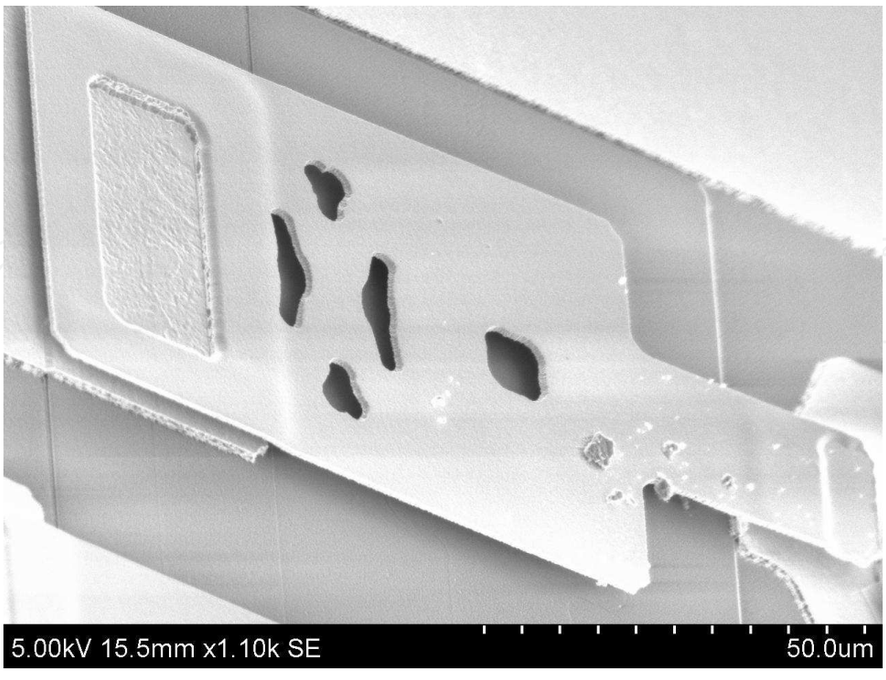

Fig. 18. SEM of fabricated novel RF MEMS switch

Figure 18 shows another design of switch which has a standard cantilever with dimensions of 80µm×60µm at the rear and an extended cantilever at the front with 40µm×20µm. Some metal particles can be seen on front portion of the cantilever which came after testing of the device while dragging the probe for contact.

8. Experimental results

The measurement setup for actuation voltage and RF performance was employed using two test configurations, i.e, preliminary screening and RF characterization. Preliminary screening was made using Cascade Microtech 10000 probe station with Tungsten needle connected to a Sony Tektronix 370 Programmable Curve Tracer. No RF performance was analyzed at this stage. The curve tracer was programmed to 0-100V DC signal with a step of 2V increment. The switches actuated at 19V and 23V. At this stage, the contact confirmation was made between two surfaces while measuring the contact resistance.
For RF performance, a two port on wafer measurement of the RF MEMS switches was performed using HP-8510 vector network analyzer (VNA) from 0-40 GHz. A Cascade Microtech 10000 probe station was used. RF probing was done using Cascade Microtech GSG RF probes with a pitch of 100µm. The SOLT (short-open-line-through) method was used for the calibration of the system before each test sequence.
An HP 4140 DC voltage source was used to actuate the switch during RF characterization. The actuation voltage for the RF MEMS switches was applied between the cantilever beam and the lower actuation pad. Two Picosecond Pulse Labs 5590 DC blocks were connected between VNA and RF cables connected with RF probes.

8.1 Electrical performance

A two port on wafer measurement of the RF MEMS switches have been performed from 0-40 GHz. When our switches were unactuated and beam was in up position, switches were in OFF state.When switches were actuated and the beam was pulled down, switches were in ON state.

8.1.1 Isolation

In order to determine the RF performance of the switch the insertion loss, return loss and isolation of the switches were measured. Isolation of the switch was measured when signal was in OFF state. Figure 19 and 20 illustrate the measured S-parameters for Design-1 and Design-2 respectively. As shown, Design-1 had an isolation of 28dB at 20GHz and better than 23dB at 40GHz. For Design-2, the isolation of the switch was 30dB at 20GHz and better than 28dB at 40GHz.

8.1.2 Insertion loss and return loss

The return loss and insertion loss of the switches were measured when signal passed through the ON state. Design-1 has a return loss better than 22dB at 20GHz and 19dB at 40GHz, for Design-2 it was better than 20dB at 20GHz and 18dB at 40GHz. This reveals good impedance matching to 50Ω of our RF MEMS designs.
Insertion loss for Design-1 was 0.75dB at 20GHz and 1.15dB at 40GHz where as insertion loss for the Design-2 was 0.8dB at 20GHz and 1.3dB at 40GHz. Higher insertion loss was

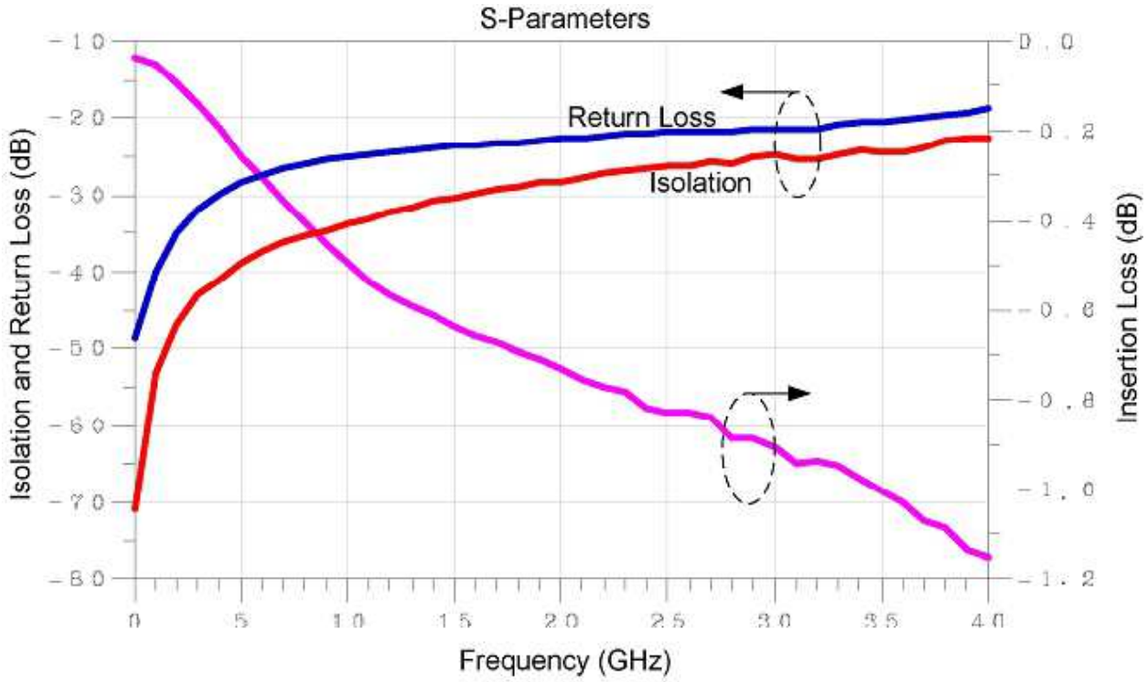

Fig. 19. Measured S-parameters of the switch using Design-1

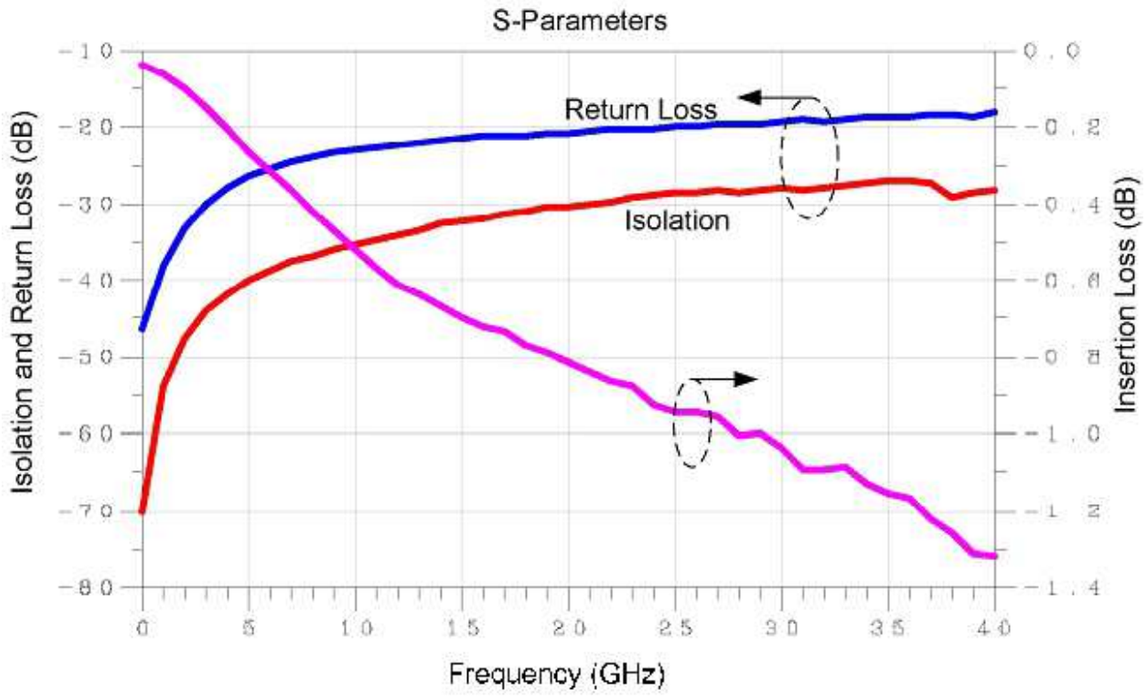

Fig. 20. Measured S-parameters of the switch using Design-2

attributed to following reasons. First, the higher contact resistance was achieved which was due to high surface roughness of the metal surface and smaller contact area. The surface roughness value is 18nm for dimple and 22nm for signal line contact area which showed that surfaces of both contact points are quite rough.

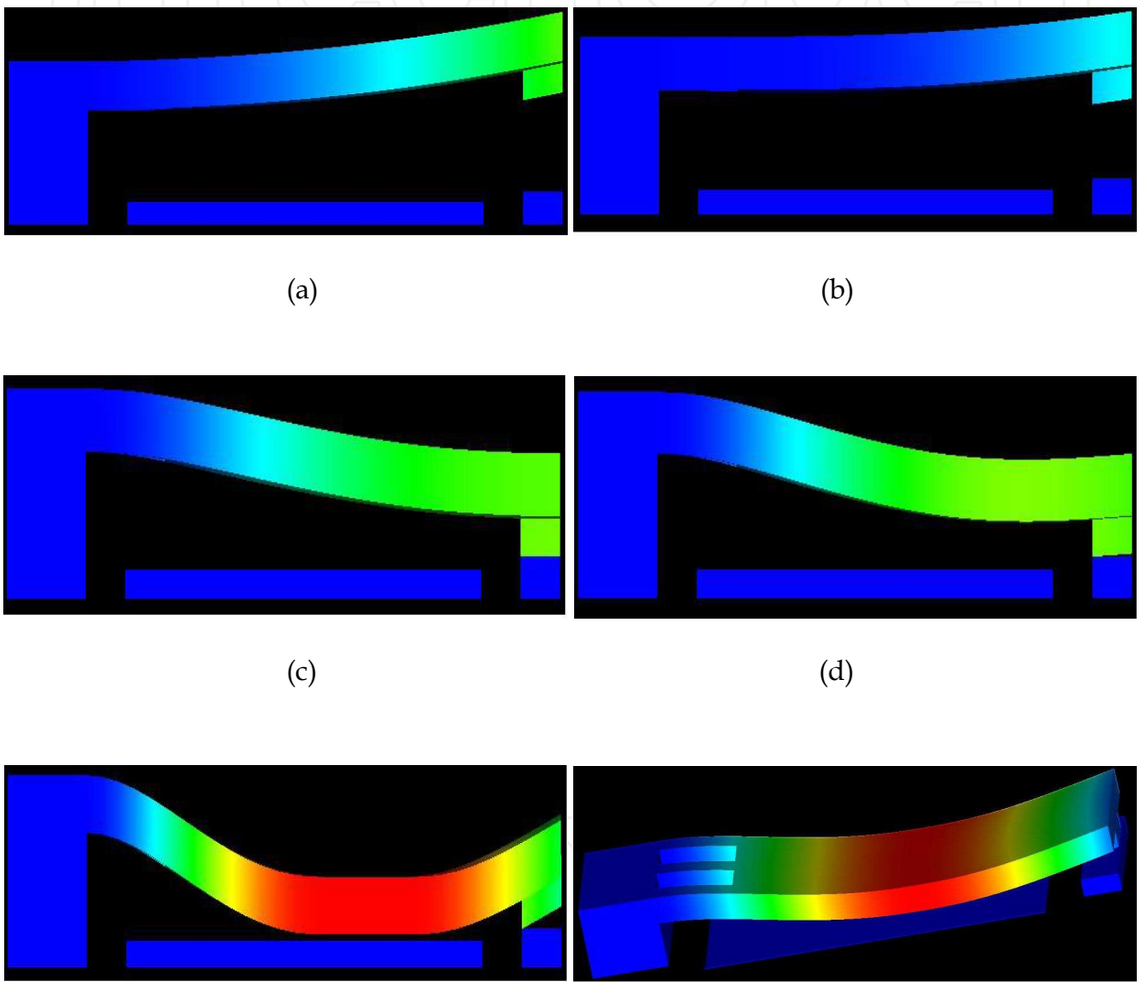

(a) (b)

(c) (d)

(e) (f)

Fig. 21. Simulated view of dimple contact during different stages of actuation

Secondly, dimple surface might have an uneven surface contact with signal line contact area. To validate this observation, a simulation test was conducted to see the dimple movement in different stages of the actuation. Figure 21 showed the movement of the cantilever beam with dimple in different stages when actuation bias was applied. The dimple made a perfect smooth contact with lower contact surface as shown in figure 21(c)

but at this point full boundary conditions were not enforced. When boundary condition were fully enforced and beam was placed in the hold down position the complete surface of dimple was not in contact and front surface of dimple has lifted up as shown in figure 21(e). This phenominon lead to higher insertion loss.

8.1.3 Actuation voltage

The measured actuation voltage of the Design-1 is 19V and Design-2 is 23V. A number of release holes can be observed in the fabricated switches. The effect on electrostatic force due to release holes had already been rationalized with inclusion of 40% of fringing field effect during simulation of spring constant of the beam designs (Rebeiz, 2003).

9. Conclusion

Bulk and surface micromachining are the two most widely used techniques for fabrication of MEMS devices. Wet and dry etching is used to achived the final release of the MEMS devices. However, in surface micromachining a combination of wet and dry etching techniques is used. Pros and cons of both the techniques have been disscused in the chapter. In wet etching capilary forces developed during the process leads to stiction and permanent adhesion of the MEMS devices. To eliminate the chance of stiction and permanent adhesion between the two solid surfaces, an inter-solid surface adhesion reduction is required. The textured surfaces and posts approach has been used for to eliminate the inter-solid surface adhesion. This was done firstly, by introducing a dimple as a supporting post between two solid surfaces and secondly, by reducing the contact area between the two metal surfaces. Both the methods were used to design improved switches which include the stiction mitigation structures. In dry etching, a dry release method with better solution for release of RF MEMS structures has been used. The technique was developed using RIE instead of CO_2 dryer or critical point drying technique. This process may lead to long term storage of the MEMS devices. Finally, fabricated novel switches have been presented validating the developed fabrication process.

A six mask all metal fabrication process was used for fabrication of RF MEMS switches. The experimental RF performance of the two fabricated swithes achieved a measured actuation voltages of 19V and 23V, respectively. Both switches showed good RF performance. Design-1 exhibited an isolation of 28dB at 20GHz and better than 23dB at 40GHz whereas, Design-2 exhibited an isolation of 30dB at 20GHz and better than 28dB at 40GHz. Both RF MEMS designs showed good impedance matching to 50Ω as deducted from the ON state S-parameter measurements. A return loss better than 22dB at 20GHz and 19dB at 40GHz was measured for Design-1 whereas, Design-2 exhibited a return loss of better than 20dB at 20GHz and 18dB at 40GHz. The insertion loss was 1.15dB and 1.3dB respectively, for all frequency band of interest.

10. Acknowledgment

This research was carried out at Centre for Quantum Computer Technology (CQCT) Micro Fabrication Laboratory, University of New South Wales (UNSW), Australia. The author wishes to thank Professor Rodica Ramer for continuous support and supervision during the

whole research The helpful advice by Dr Eric Gauja during the fabrication is greatly appreciated.

11. References

Abe, T.; Messner, W. C. & Reed, M. L. (1995). Effective Methods to Prevent Stiction during Post Release Etch Processing, *Proceedings of International Conference on Micro Electro Mechanical Systems (IEEE MEMS 95)*, pp. 94-99, ISBN 0-7803-2503-6, 29th Jan – 2nd Feb 1995. Netherland

Alley, R. L.; Cuan, G. J.; Howe, R. T. & Momvopoulos, K. (1992). The Effect of Release Etch Processing on Surface Microstructure Stiction, *Proceedings of IEEE 5th Technical Digest on Solid State Sensors and Actuators Workshop*, pp. 202-207, ISBN 0-7803-0456-X, 22-25 June 1992, SC, USA

Campbell, S. A. (1996). *The Science and Engineering of Microelectronic Fabrication*, Oxford University Press, ISBN 0-19-510508-7, New York USA

Chan, K. Y.; Daneshmand, M.; Mansour, R. R. & Ramer, R. (2007). Novel Beam Design for Compact RF MEMS Series Switches, *Proceedings of Asia Pacific Microwave Conference (APMC 2007)*, pp. 229-232, ISBN 978-1-4244-0749-4, 11-14 Dec 2007, Bangkok Thailand

Forsen, E.; Davis, Z. J.; Dong, M.; Nilsson, S. G.; Montelius, L. & Boisen, A. (2004). Dry Release of Suspended Nanostructures, *Journal of Microelectronic Engineering*, No. 73-74, pp. 487-490, doi: 10.1016/j.mee.2004.03.022, ISSN 0167-9317

Harsh, K. F.; Zhang, W.; Bright, V. M. & Lee, Y. C., (1999). Flip Chip Assembly for Si Based RF MEMS, *Proceedings of 12th International Conference on Micro Electro Mechanical Systems (IEEE MEMS 99)*, pp. 273-278, ISBN 0-7803-5194-0, 17-21 Jan 1999, Orlando, FL USA

Israelachvili, J. N. (1991). *Intermolecular and Surface Forces,* Academic Press Ltd, ISBN 0-12-375181-0, London UK

Madou, M. J. (2002). *Fundamentals of Microfabrication,* pp. 276-277, CRC Press, Florida, ISBN 0-8493-0826-7, USA

Mastrangelo, C. H. (2000). Suppression of Stiction in MEMS, *Proceedings of Material Research Society Symposium*, Vol. 605, pp. 105-116

Mastrangelo, C. H. & Hsu, C. H. (1993). Mechanical Stability and Adhesion of Microstructures under Capillary Forces – Part I: Basic Theory, *Journal of Microelectromechanical Systems*, Vol. 2, No. 1, pp. 33-43, ISSN 1057-7157

Mastrangelo, C. H. & Hsu, C. H. (1992). A Simple Experimental Technique for Measurement of the Work of Adhesion of Microstructures, *Proceedings of IEEE 5th Technical Digest on Solid State Sensors and Actuators Workshop*, pp. 2008-2012, ISBN 0-7803-0456-X, SC, USA

Orpana, M. & Korhonen, A. O. (1991). Control of Residual Stress of Polysilicon Thin Films by Heavy Doping in Surface Micromachining, *Proceedings of International Conference on Solid State Sensors and Actuators Transducers 91,* Vol. 23, pp. 957-960, ISBN 0-87942-585-7, 24-27 June 1991, San Francisco, CA USA

Rebeiz, G. M. (2003). *RF MEMS : Theory Design and Technology,* John Wiley and Sons Ltd, ISBN 0-471-20169-3, New York USA

Varadan, V. K.; Vinoy, K. J. & Jose, K. A. (2003). *RF MEMS and Their Applications*, John Wiley and Sons Ltd, ISBN 0-470-84308-X, New York USA

IntechOpen

IntechOpen

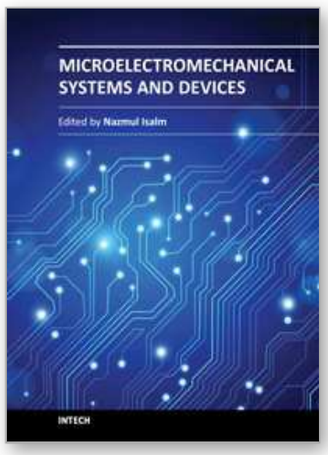

Microelectromechanical Systems and Devices

Edited by Dr Nazmul Islam

ISBN 978-953-51-0306-6
Hard cover, 480 pages
Publisher InTech
Published online 28, March, 2012
Published in print edition March, 2012

The advances of microelectromechanical systems (MEMS) and devices have been instrumental in the demonstration of new devices and applications, and even in the creation of new fields of research and development: bioMEMS, actuators, microfluidic devices, RF and optical MEMS. Experience indicates a need for MEMS book covering these materials as well as the most important process steps in bulk micro-machining and modeling. We are very pleased to present this book that contains 18 chapters, written by the experts in the field of MEMS. These chapters are groups into four broad sections of BioMEMS Devices, MEMS characterization and micromachining, RF and Optical MEMS, and MEMS based Actuators. The book starts with the emerging field of bioMEMS, including MEMS coil for retinal prostheses, DNA extraction by micro/bio-fluidics devices and acoustic biosensors. MEMS characterization, micromachining, macromodels, RF and Optical MEMS switches are discussed in next sections. The book concludes with the emphasis on MEMS based actuators.

How to reference

In order to correctly reference this scholarly work, feel free to copy and paste the following:

Hamood Ur Rahman (2012). Plasma Based Dry Release of MEMS Devices, Microelectromechanical Systems and Devices, Dr Nazmul Islam (Ed.), ISBN: 978-953-51-0306-6, InTech, Available from: http://www.intechopen.com/books/microelectromechanical-systems-and-devices/plasma-based-dry-release-of-mems-devices

INTECH
open science | open minds

InTech Europe
University Campus STeP Ri
Slavka Krautzeka 83/A
51000 Rijeka, Croatia
Phone: +385 (51) 770 447
Fax: +385 (51) 686 166
www.intechopen.com

InTech China
Unit 405, Office Block, Hotel Equatorial Shanghai
No.65, Yan An Road (West), Shanghai, 200040, China
中国上海市延安西路65号上海国际贵都大饭店办公楼405单元
Phone: +86-21-62489820
Fax: +86-21-62489821

© 2012 The Author(s). Licensee IntechOpen. This is an open access article distributed under the terms of the Creative Commons Attribution 3.0 License, which permits unrestricted use, distribution, and reproduction in any medium, provided the original work is properly cited.

IntechOpen

IntechOpen